EXPERIMENTAL AND NUMERICAL STUDIES OF A DC MICRODISCHARGE PLASMA THRUSTER

U. KC, T. Deconinck, P. L. Varghese, and L. L. Raja

ASE-EM Department,The University of Texas at Austin, Austin, Texas 78712, USA

ABSTRACT

We have designed a simple Microdischarge Plasma Thruster (MPT) for small satellite propulsion, and studied it by performing experiments and running simulations in a numerical model. The MPT comprises a tri-layer sandwich structure with a dielectric layer sandwiched between two electrode layers, and a contoured through-hole drilled into the structure. Each layer is a few hundred microns thick and the hole diameter is also approximately this size. The device operates at Ar flow rates of ~1 *sccm* with modest electrode voltages (~1000 *V*). Spectral measurements of the plume are used to determine its composition and calculate the electronic excitation temperature. A two-dimensional computational model has been developed to provide a detailed description of the plasma dynamics inside the MPT including power deposition, ionization, coupling of the plasma phenomena with high-speed flow, and propulsion system performance. Gas heating, primarily due to ion Joule heating, is found to have a strong influence on the overall discharge behavior.

INTRODUCTION

Small satellites (mass less than 100 kg) have recently gained interest for various commercial, military, and science space missions [1-2]. These satellites are power-limited: typically <1 W/kg of spacecraft mass is available. Propulsion requirements can vary significantly, but are generally characterized by their very low thrust values (~ mN) and low impulse bits for attitude control (~10 μN-s). Scaling traditional propulsion systems down in power and size to suit the needs of small satellites is a major engineering challenge.

The extremely small dimensions of microdischarges combined with intense and controllable gas heating can be exploited in microthrusters technologies. Like conventional cold gas thrusters, electrothermal microdischarge propulsion systems can have extremely low mass and volume footprints. The microdischarge operates in an abnormal glow mode with positive differential resistivity. An increase in input electrical power results in almost linear increase in the gas temperatures; this property of microdischarges is a key feature that can be exploited in the MPT concept. The thrust from these devices is widely tunable by varying power levels.

EXPERIMENTAL STUDIES

Figure 1 shows the schematic of a prototype MPT used in the experimental studies. The MPT has a multilayer sandwich structure. It has three electrodes- e_1, e_2, e_3 which are ~ 100 μm thick and they are separated by ~200 μm thick dielectrics. It has a narrow duct ~100 μm in diameter which expands to ~330 μm downstream of the throat. From gas dynamic point of view the cavity inside the MPT resembles a converging diverging nozzle that can accelerate the gas to super sonic velocities downstream of the throat. The mass of the assembled piece is 0.9 g and the total thickness is about 1.1 mm.

The discharge is generated between e_1 and e_3. It heats the neutral gas which accelerates as it flows in the converging diverging nozzle. The ion flow is also accelerated by the nozzle and the floating potential that exists between the MPT and the vacuum. The expulsion of hot gas and ions into the vacuum generates thrust. The MPT has potentially important advantages over competing concepts such as the micro resistojet thruster [3], which also relies on preheating an expanding gas stream. The important difference between a resistojet and the MPT is the nature of power deposition into the gas. In a resistojet, the heating element is essentially the hottest part of the system and heat addition to the gas occurs via conduction/convection to the gas stream. There is clearly an upper limit on the heating

element temperature which in turn limits the amount of heat delivered to the gas. In the MPT, the gas is heated directly by the plasma. Importantly, if the plasma thermal power deposition occurs far away from the surfaces, much higher thermal energies can be delivered to the gas. So far the MPT has been operated using argon. When the argon flow rate is 5 sccm, the pressure in the cavity ranges from ~100 Torr upstream to ~1 Torr near the exit. Between e_2 and e_3, because the number density of gas species (N) is low, the ratio of characteristic electric field strength (E) to the number density of neutral species E/N is high. This is favorable to enhance ionization process in the discharge. Ordinarily, at pressures as low as ~1 Torr and linear dimensions of the order of few hundred microns, the break down voltage is in the order of several kV if the discharge is to be sustained only by secondary electron emissions at the cathode. The structure of the MPT helps to overcome such high voltage requirement to sustain the discharge. The high pressure (~100 Torr) between e_1 and e_2 helps to reduce the break down voltage of gas inside the MPT. The region of the discharge between e_1 and e_2 can also supply electrons to the region between e_2 and e_3 to increase and sustain ionization process in that region. In this way, MPT can be stably operated using a non corrosive/ non contaminating propellant at relatively low voltages.

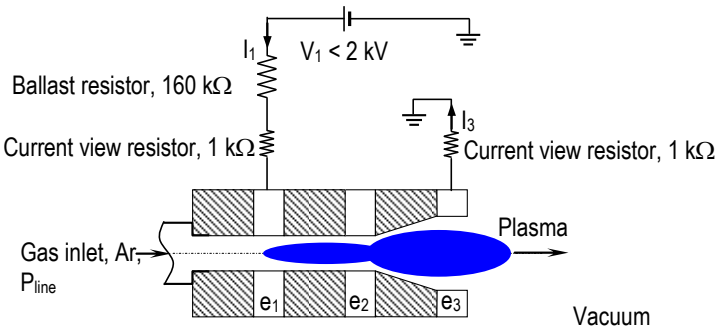

Fig. 1 Schematic diagram of MPT with electrical circuit used in the experiments

An ion probe was used to determine ion distribution in the plume. The probe consists of a copper rod of radius 1 mm inserted into a glass tube that has 1 mm thick wall. The probe surface is biased at -100 V and is mounted on a linear translation feed through so that it can traverse perpendicular to the plume axis on the horizontal plane. The probe is 4.4 cm from the MPT exit when aligned with the plume axis. Figure 2a shows a photograph of the experimental set up with the probe in place. Figure 2b shows the MPT in operation. It is a highly under-expanded jet as the pressure at the exit is ~1 Torr and the pressure in the vacuum chamber is ~10^{-3} Torr.

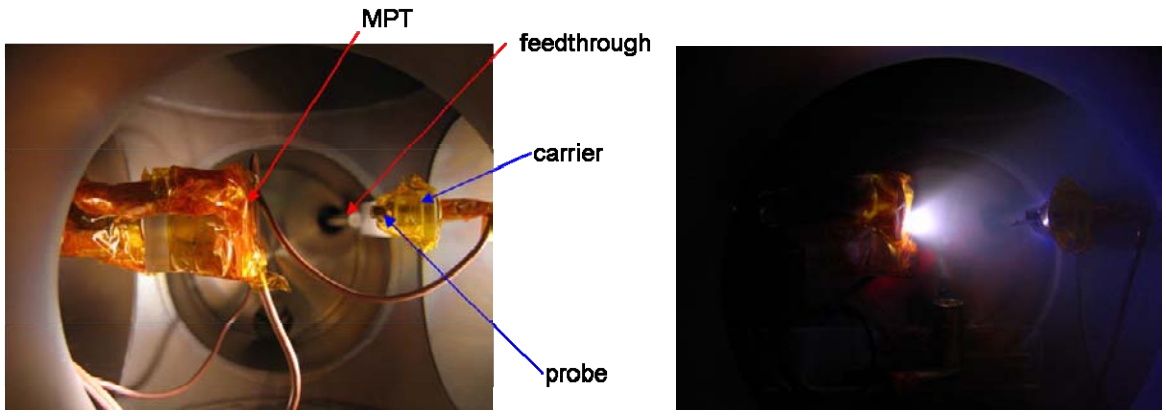

Fig. 2. (a) MPT mounted inside the vacuum chamber with ion probe; (b) MPT in operation

Figure 3a shows the power to the MPT as a function of supply voltage and flow rate. Typical operating power is between 50 and 500 mW. The power is seen to increase with flow rate at a fixed supply

voltage. This implies that at higher flow rates the increase in the number density of charge carriers outweighs the increase in collision frequency.

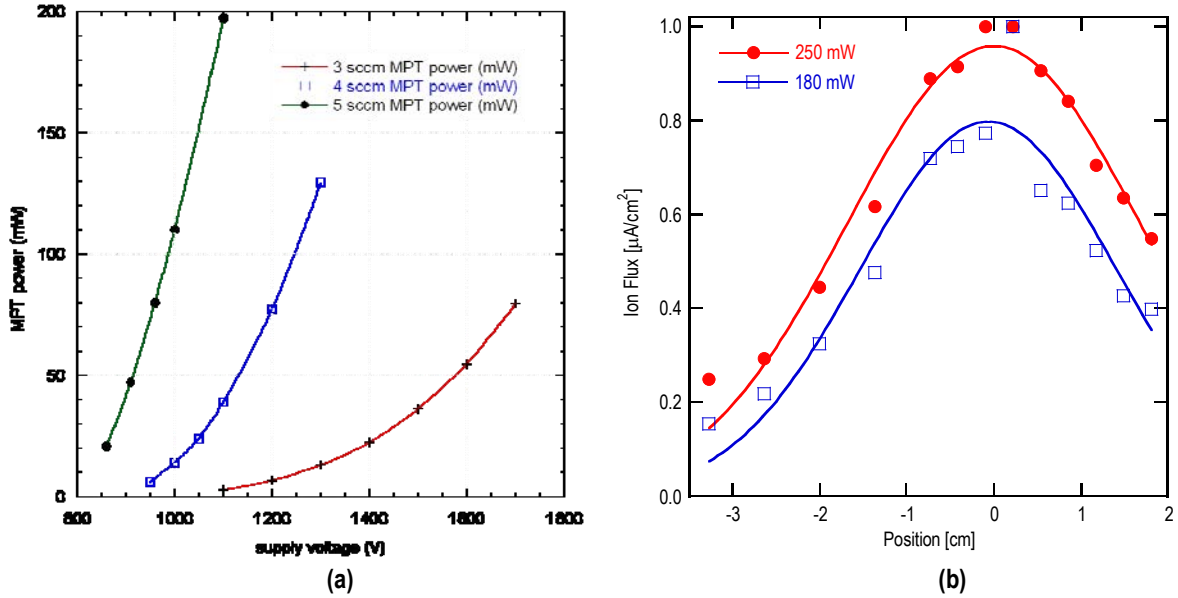

Fig. 3 (a) Variation of power with voltage at several flow rates through the MPT (b) Ion current distribution in the plume

Figure 3b shows some results of the ion probe measurements. The total ion current in the plume is estimated from an analytic integral of a Gaussian fit to the probe data. For example, the total ion current at 250 mW discharge power is 17.0 μA. Assuming that all the ions are Ar^+, the ratio of ion fraction in the plume is 5.2×10^{-5}. Assuming that all the ions in the discharge are also Ar^+, the ratio of ion current in the plume to discharge current is 5.6×10^{-2}. The low ion fraction implies that ion acceleration will not contribute significantly to the device thrust which comes mainly from gas dynamic expansion.

Emission spectroscopy was used to characterize the plume emerging from the MPT. Light from the plume was focused onto an optical fiber (diameter 600 μm) and transmitted to a 0.25 m spectrograph with an entrance slit width of 200 μm, and a grating with 1800 grooves/mm. The spectra were recorded on a spectrograph with a CCD array detector; the exposure time ranged from 600 ms for the strongest lines, up to 60 s for weaker lines. The spatial extent of the probe volume was determined by probing emission from an argon calibration lamp focused into a pinhole that had a diameter of 100 μm. The depth of field was found to be 3.03 cm and the imaged region along the plume axis was 260 μm. The plume spectra were recorded from the region 2 mm downstream of the exit plane. At this location the length of the visible plume perpendicular to its axis is estimated to be less than 3 cm so the optical system collects light over the entire depth of the plume in these emission measurements.

The fixed pattern noise on the detector was subtracted and the detector and optical system response in the range 400-900 nm was calibrated with a black body source at 1473 K. Spectral lines from Ar, Ar^+, and Mo (from electrode erosion) were observed. Figure 4a is a sample spectrum showing a total of 14 lines from neutral Ar with detectable intensity in this spectral range (not all the lines are apparent in the figure). The absolute positions and spectroscopic data on the lines were taken from the NIST on-line atomic data base [4]. The individual line intensities are determined by fitting Doppler profiles to the spectral data. The fitted line positions agree very well with the NIST data with a constant small offset of 0.827 nm (arising from a small offset in the spectrometer wavelength calibration) providing confidence that the lines are assigned correctly. Using data on neutral Ar lines in ±20 nm wavelength intervals around 710 nm and 811 nm, we constructed a Boltzmann plot to determine the excitation temperature of the electronic states of Ar. The results of this analysis are shown in Fig. 4b. The error bars shown

correspond to ±15% and are principally due to the estimated uncertainty of the Einstein A coefficients for these transitions. The NIST on-line data base quotes the absolute accuracy of the Einstein A coefficients for the observed transitions as C (<±25%) or D+(<±40%) [4]. Our estimate of ±15% is based on the assumption that the *relative* precision of the data is somewhat better than the *absolute* accuracy. The measurements are consistent with an "excitation" temperature of approximately 0.66 eV (7650 K). This is very different from the gas kinetic temperature which is expected to be ~1000 K. Note that the gas temperature could not be determined from the recorded spectral line shape as the measured line shape is determined largely by the spectrometer resolution. The excitation temperature of these electronic states in the plume is not expected to be representative of the electron temperature in the discharge inside of the MPT which is probably several eV. It is possible that the result represents the free electron temperature in the weakly ionized plume, but the measurements must be interpreted with caution as they represent emission from high lying excited states of neutral Ar; as seen in Fig. 4b the emitting states are 13-15 eV above the ground state. Hence electron impact ionization of these states would be from electrons at the high energy tail of the energy distribution which is likely to be depleted and out of equilibrium with the majority of the distribution.

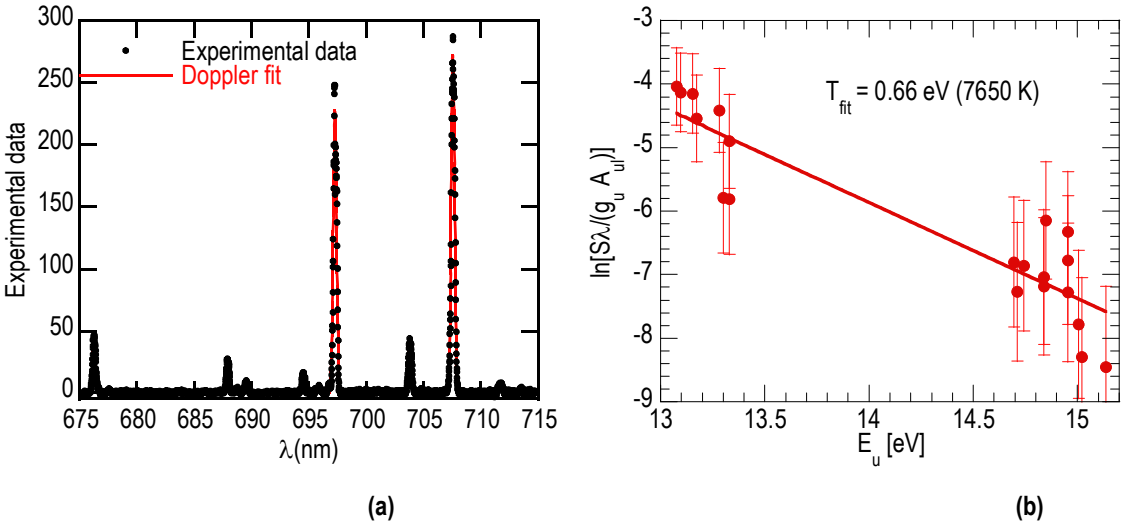

(a) **(b)**

Fig. 4 (a) Experimental spectrum and fit to Doppler line shape; (b) Boltzmann plot based on fitted line intensities

NUMERICAL STUDIES

In the MPT, the microdischarge plasma is in a highly non-equilibrium state with disparate electron and gas temperatures and non-equilibrium finite-rate chemical effects. The gas flow is characterized by low-Reynolds number viscous dominated effects combined with high Mach number compressibility effects owing to the expansion of the relatively high-pressure (~100 Torr) micronozzle gas stream into vacuum. Both the plasma and flow phenomena are strongly coupled: the plasma causes gas heating, which modifies the gas density, and hence the flow field; the gas flow velocities, in turn, affects the distributions species and temperature of plasma in the discharge. The integrated plasma-flow model used in this study is described in detail in [5].

A pure argon plasma gas chemistry [6, 7] is used which comprises six species: electrons (e), atomic argon ions (Ar^+), molecular argon ions (Ar_2^+), electronically excited atoms (Ar^*), electronically excited molecules (Ar_2^*), and the background argon atoms (Ar). Dimer species are included because of the relatively high pressures in the upstream section of the micronozzle (~100 Torr). At solid surfaces all excited species and charged species are assumed to get quenched with unity sticking coefficient. Upon quenching at surfaces, each dimer ion and excited species is assumed to return to plasma as a pair of ground state neutral Ar atoms, while the monomer species return as single Ar atoms.

Conservation equations for the gas mass density, mass-averaged gas velocity, and the gas energy are solved using compressible Navier-Stokes equations in axisymmetric form. The flow solution influences the plasma discharge through the pressure, temperature and velocity fields appearing in the plasma governing equations. On the other hand, electrostatic forces and electrothermal heating act as external body forces and external heat source, respectively, in the Navier-Stokes equations. The Joule heating terms appearing in the electron energy equation are evaluated using a species flux reconstruction approach [8].

Both the plasma governing equation and the compressible flow Navier-Stokes equations are spatially discretized using a cell-centered finite volume approach on an unstructured mesh with mixed mesh cell types. A steady state solution is sought in all cases. Both the plasma and flow governing equations are solved as transient problems with time-stepping of the solution to a steady state. The plasma governing equations are solved using an implicit time-discretization approach with local linearization of the governing equations at each time step. For the flow governing equations, the inviscid flux terms are evaluated with the Advection Upstream Splitting Methods (AUSM) [9] and the viscous flux terms are evaluated using the Haselbacher approach [10] The flow equations are also solved using implicit time-discretization, with a dual-time stepping approach to iteratively solve for the solution at each time step. The viscous terms in the flow equations require computation of the solution variable gradients at cell centers. We use a Green-Gauss method to reconstruct these gradients based on cell-centered values of these variables. Finally, the compressible flow can develop shock discontinuities. The Venkatakrishnan flux limiter approach [11] is used to stabilize and produce monotone solutions in the presence of such discontinuities.

Figure 5 shows the geometry of the MPT used for the simulations. The geometry consists of an axisymmetric constant area “pipe” section of 500 μm length, followed by a diverging section that is 200 μm in length, which is terminated by a 150 μm long constant area section. The radius of the upstream constant area pipe section is 50 μm, and the exit section is 150 μm in radius. The ring shaped electrodes have an axial thickness of 150 μm, while the dielectric layer has an axial thickness of 550 μm. The mesh consists of about 3600 cells, which includes a combination of triangles and quadrilaterals.

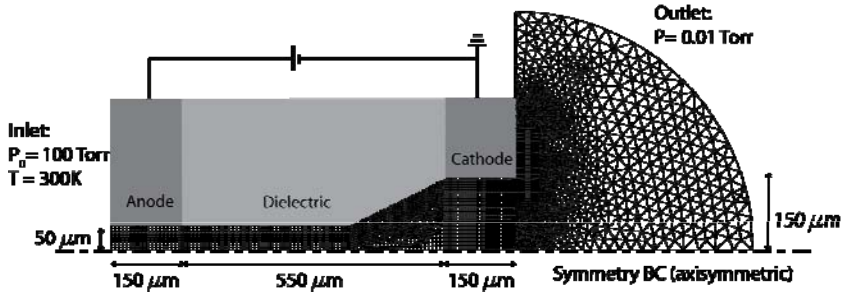

Figure 5. Schematic of the MPT device and computational mesh. The geometry is cylindrically symmetric.

The flow direction is from left to right in Fig. 5. The flow enters the constant area pipe section on the left and exits the domain along the curved (arc-shaped) boundary on the right. Four boundary sections are not modeled as solid walls for the gas discharge governing equations. Zero-flux boundary conditions are imposed at the boundary section formed by the symmetry axis. For numerical stability reasons, zero-flux boundary conditions are also used for the gas discharge governing equations at the inlet and outer cathode surface boundaries. These boundaries are sufficiently away from the main discharge region and do not influence the results. The far-field boundary on the right side of the computational domain is modeled as an “outflow” boundary, where the plasma variables (species number densities and electron energy density) are convected away by the gas flow, while zero-flux boundary conditions are imposed for the Poisson’s equation. The value of the plasma variable from the adjacent interior cell is used to interpolate the flux at this far-field boundary. The power input is provided by applying a fixed

positive DC voltage at the anode (without ballast resistance), while the cathode is grounded. For all the calculations shown here the secondary electron emission coefficient is set at a value of 0.03, corresponding to a nickel surface interacting with an argon plasma [12].

The inlet total (stagnation) pressure is 100 Torr (for the base case), and a small but non-zero outlet pressure (0.05 Torr) is required to stabilize the numerical scheme in the "vacuum" part of the domain. The inlet gas static temperature is fixed at 300 K. The solid wall temperatures are fixed at 300 K. The inlet flow velocity is computed self-consistently using the inlet conditions, the inlet static pressure extrapolated from the interior of the domain, and isentropic expansion relations. No-slip boundary conditions are applied at solid walls for the momentum equation. The Knudsen numbers for the flow are sufficiently low over much of the MPT device length (about 0.01 at the inlet to about 0.08 at the exit plane) that slip-flow and wall-temperature jump boundary conditions are not necessary. This has been verified by running simulations with the appropriate jump boundary conditions.

Table I lists discharge conditions for which results are presented here. The effect of other parameters was also studied and more detailed results are given in Ref 5. For the base case, the discharge voltage is set to 750 V, and the computed discharge current is 0.87 mA. The stagnation pressure (100 Torr) and static temperature (300 K) imposed at the inlet determine the inlet velocity which is computed at about 100 m/s corresponding to a flow rate of 5.2 sccm. Representative plasma properties at steady state for this case are shown as false color images in Fig. 6. The space charge density is high enough that the bulk plasma extends well into the diverging part of the micronozzle creating a hollow-cathode-like annular cathode sheath. Under these operating conditions, the cathode sheath is about 100 μm thick (see electrostatic potential in Fig. 6a), occupying a significant fraction of the total discharge volume. In the cathode fall, the potential drops by nearly 750 V over ~100 μm producing a characteristic field strength of ~75 kV/cm and a reduced electric field (E/N) of ~10^5 Td (Townsend). Electron density contours are presented in Fig. 6b and show two local maxima. The first peak is inside the constant area pipe section (~$7\text{x}10^{19}$ m^{-3}), and the second higher peak is in the diverging section of the nozzle (~$3\text{x}10^{20}$ m^{-3}). The well-defined cathode sheath structure observed in Fig. 6a is apparent in the density contours with an abrupt drop in the electron densities in the diverging micronozzle section. The MPT discharge clearly operates in the glow discharge mode rather than the Townsend/predischarge mode. The electron temperatures are displayed in Fig. 6c. The electron temperature is only shown in regions of the discharge where the electron number density is greater than 3×10^{17} m^{-3}, i.e. 10^{-3} of the peak value of the electron number density. The electron energy content is negligible in the rest of the domain. The electron temperature remains nearly uniform (~2 eV) in the bulk plasma over most of the constant area pipe section, and gradually increases in the diverging section of the devices to temperatures around 3 eV at the cathode sheath edge.

Case	Inlet total pressure (Torr)	P D (Torr cm)	Flow rate (sccm)	Voltage (V)	Current (mA)	Power (mW)	Computed thrust (μN)	Computed power (mW)
Base case	100	5.5	5.2	750	0.87	650	100	650
Larger power input	100	5.5	5.2	1000	1.8	1800	128	1800
Higher cathode temperature	100	5.5	5.2	750	0.72	540	112	540

Table I. Operating conditions considered for the results presented in this work. The characteristic discharge dimension *D* is taken to be the thickness of the dielectric layer located between the electrodes (550 μm) and the characteristic pressure is taken to be the inlet total pressure.

The electron generation rate in the discharge through gas-phase reactions is shown in Fig. 6d. Significant generation of electrons is observed over the entire micronozzle with maximum generation observed in the diverging section. This location corresponds to a relatively higher electron temperature (~3 eV) and reasonably high background densities in the expanding gas flow. The argon monomer ion

(Ar^+) and dimer ion (Ar_2^+) number densities are shown in Figs. 6e and 6f respectively. Atomic argon ions constitute the dominant ion species in the microdischarge. High background densities favor three-body reactions that forms dimer species. Therefore, most dimer ions are located in the constant area pipe section, where the pressure is relatively high. The dielectric surfaces support a net negative charge owing to electron trapping which in turn supports a positive sheath over the entire dielectric length between the anode and the cathode. This is apparent from the excess of positive ions compared to electrons, just above the dielectric surfaces. The net negative charge at the dielectric enforces the electron wall flux to equal the total positive ion wall flux (at steady state), so no net current is drawn through the dielectric surfaces.

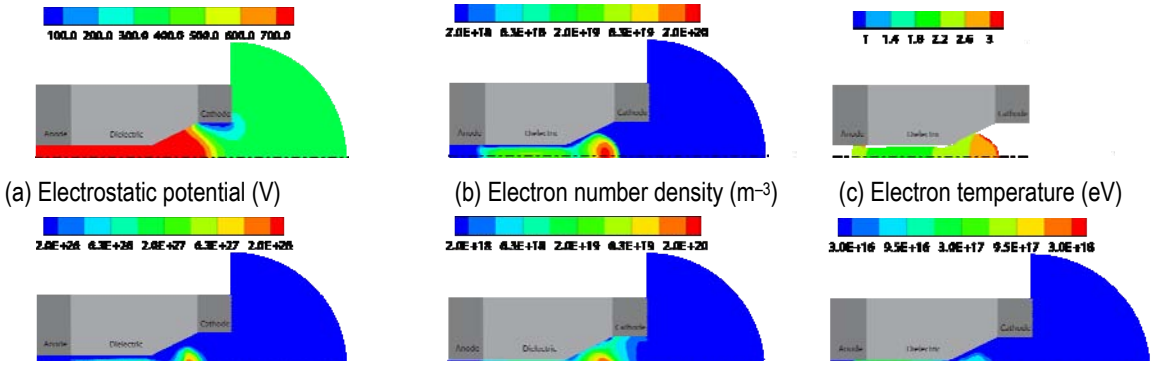

(a) Electrostatic potential (V) (b) Electron number density (m^{-3}) (c) Electron temperature (eV)

(d) Electron generation rate ($m^{-3}\,s^{-1}$) (e) Ar^+ number density (m^{-3}) (f) Ar_2^+ number density (m^{-3})

Fig. 6 Plasma properties in the MPT. The inlet total pressure is 100 Torr (13.3 kPa) and the mass flow rate is 5.2 sccm. The applied potential difference between the electrodes is 750 V and the power input is 650 mW

Figure 7 shows the effects of power input on discharge characteristics and flow properties. Results are presented for the base case, where the discharge voltage is fixed at 750 V and the discharge power is 650 mW, and for a case where the discharge voltage is fixed at 1000 V with a corresponding power of 1800 mW. In both cases, the inlet total pressure is 100 Torr and the flow rate is 5.2 sccm.

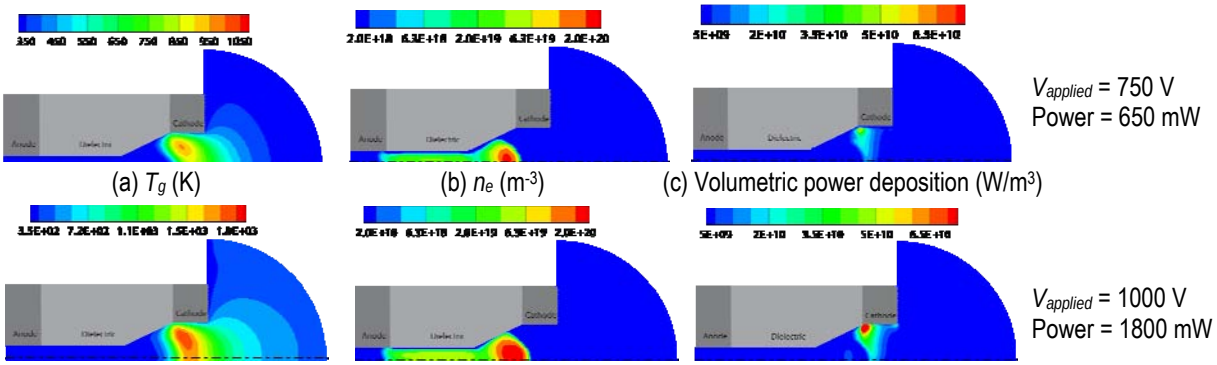

(a) T_g (K) (b) n_e (m^{-3}) (c) Volumetric power deposition (W/m^3)

Fig. 7 Effect of applied voltage and discharge power on (a) gas temperature, (b) electron density and (c) volumetric power deposition in the MPT

Gas temperatures are compared in Fig. 7a. The peak temperature for the high power case is 1850 K compared to 950 K for the base case. Figure 7b shows that the plasma is more intense for higher power inputs, i.e. the ionized species number densities are higher. Electron number densities increase by a factor of ~2 as the power input increases from 650 mW to 1800 mW. Contours of the power deposition in the MPT are shown in Fig. 7c. The net power deposition into neutral gas scales almost linearly with the power input. Importantly, these results show that changing the external power input is an effective method to control the level of gas heating in the discharge, which, in turn, affects the gas temperature and the thrust produced by the device. This is a key feature of our proposed MPT concept

– the computed thrust increases to 128 μN for the high power case, which corresponds to a specific impulse of 95 s.

In practice a large fraction of the input power is lost to the walls, so the cathode temperature is expected to be significantly higher than the constant 300 K assumed in the above computations. An accurate estimate of the cathode temperature would require solving an energy balance equation for the entire MPT device (including solid materials). The effect of the cathode temperature on the MPT discharge parameters and performance is studied by comparing the base case solution to a case where the cathode temperature is fixed at 1000 K. All other conditions are kept the same as the base case. Figure 8a shows the gas temperature contours for the two cases. As might be expected, the spatial distribution of computed gas temperature is strongly dependent on the assumed cathode temperature. The peak gas temperature reaches 1150 K with the cathode temperature fixed at 1000 K, compared to 950 K for the base case, and the region of high gas temperatures occupies a larger fraction of the MPT volume than for the base case. Increasing the cathode temperature reduces the temperature gradients at the cathode surface, thereby decreasing the net thermal loss.

The axial velocity contours are shown for the two cases in Fig. 8b. As the cathode temperature is increased, the reduced heat losses allow for an increased expansion of the gas in the diverging section of the micronozzle. The computed thrust therefore increases from 100 μN for the base case to 112 μN when the cathode temperature is 1000 K. It should be noted that the power input has decreased to a value of 540 mW at the higher cathode temperature, compared to 650 mW for the base case. The higher gas temperatures (and therefore lower background Ar densities) result in a decrease in ionization. The lower power/current can be attributed to the lower charge densities and hence to the lower plasma conductivity.

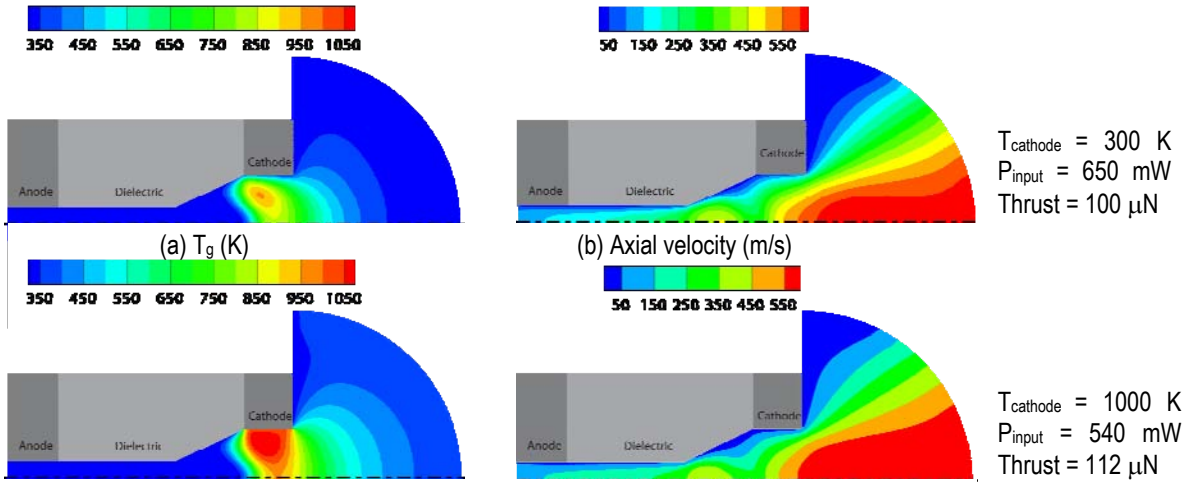

Fig. 8 Effect of cathode temperature on (a) gas temperature and (b) axial velocity

CONCLUSION

The MPT is an electrothermal micro propulsion device that was designed and studied with the goals of minimizing its size, mass, operating power and propellant consumption. The MPT was successfully operated in the lab at low flow rates of ~1 sccm. The most stable operation was obtained with the upstream electrode (e_1) as the anode, the downstream electrode (e_3) as the cathode and the middle electrode e_2 left floating. The MPT operates as an electrothermal thruster because most of the momentum thrust of the MPT is generated by the expulsion of hot neutral argon atoms. Measurements with the ion probe revealed that there is also a small fraction of ions in the plume. Hence, the MPT is able to expel ions without the use of an external magnetic field or an external electron emitter. Comparison of current voltage characteristics of the MPT (not presented here) with the ion probe measurements show that the net ion current in the plume is also considerably less than the discharge

current. The presence of ions in the plume was confirmed by emission spectroscopy. Molybdenum atoms in the plume detected from their spectra implies that the plume erodes the exposed regions of the electrodes. Using the emission spectra the electronic excitation temperature of the neutral Ar was determined to be ~0.7 eV (~7700 K). The thrust from the MPT is yet to be measured experimentally. The material selection for the electrodes also needs to be addressed in future.

A detailed computational model was also used to study microdisharge and flow interaction phenomena for micropropulsion applications. The model consists of a plasma module coupled to a flow module and is solved on a hybrid unstructured mesh framework. The plasma module provides a self-consistent, multi-species, multi-temperature description of the microdischarge phenomena while the flow module provides a description of the low Reynolds number compressible flow through the micropropulsion system.

The coupled plasma-flow simulations showed that the electrostatic component of thrust is negligible for the current MPT configuration. Electrothermal heating is due primarily to the ion Joule heating occurring near the cathode surfaces. A large part of the input power is therefore deposited into the walls rather than going to neutral gas heating. Future work must explore strategies that will allow for power deposition away from the wall, near the centerline. For example, radio-frequency operation of the microdischarge may help reduce the thermal load on the microdischarge, and increase the direct power deposition into the neutral gas.

For a discharge voltage of 750 V, a power input of 650 mW, and an argon flow rate of 5.2 sccm, the computed specific impulse of the device is 74 s, a factor of ~1.5 higher than the cold gas micronozzle. For these conditions, charged species densities on the order of 5×10^{20} m^{-3} and peak gas temperatures of ~1000 K are predicted. The microdischarge remains mostly confined inside the micronozzle and operates in an abnormal regime. Additional simulation studies on the MPT indicate that the power input has a strong influence on overall discharge properties. The net power deposition into the neutral gas scales with the power input, providing a method of controlling the gas temperature and the thrust level of the MPT. This feature constitutes an important advantage over traditional cold gas thrusters.

The sensitivity of above results to important uncertain parameters of the model has been studied. A higher cathode temperature is found to reduce the heat losses at solid walls and is beneficial for the thruster performance, though there is obviously an upper limit to avoid damage to the cathode. The cathode temperature could be determined self-consistently by solving the solid thermal conduction equation in the dielectric and electrode material to quantify the overall thermal field in the MPT device. The thermal loads from the plasma at the wall surfaces will drive heat transfer into the device structure potentially resulting in “hot spots” that can be investigated through the simulations. These coupled multi-physics simulation results would in turn provide an informed approach to the better design of the MPT.

ACKNOWLEDGEMENTS

This work was supported by AFOSR under grant FA9550-06-1-0176.

REFERENCES

1. Micci, M. M., and Ketsdever, A. D., *Micropropulsion for Small Spacecraft*, Progress in Astronautics and Aeronautics, AIAA, Reston, VA, 2000.
2. Sweeting, M. N., “Space at Surrey: micro-mini-satellites for affordable access to space,” *Air and Space Europe*, Vol. 2, 2000, pp. 38-52.
3. Coxhill, I. G., Gibbon, D., “A Xenon Resistojet Propulsion System for Microsatellites,” *Proceedings of the 41st AIAA/ASME/SAE/ASEE Joint Propulsion Conference and Exhibit*, AIAA paper 2005-4260, Tucson, AZ, 2005.
4. Ralchenko, Yu., Kramida, A.E., Reader, J., and NIST ASD Team (2008). *NIST Atomic Spectra Database* (version 3.1.5), [Online]. Available: http://physics.nist.gov/asd3 [2009, May 6]. National Institute of Standards and Technology, Gaithersburg, MD.

5. Deconinck, T., “Simulation studies of direct-current microdischarges for electric propulsion”, Ph. D. dissertation, The University of Texas at Austin, December 2008.
6. Hagelaar, G. J. M. and Pitchford, L. C., “Solving the Boltzmann equation to obtain electron transport coefficients and rate coefficients for fluid models,” *Plasma Sources Science and Technology*, Vol. 14, 2005, pp. 722-733.
7. Lay, B., Moss, R. S., Rauf, S., and Kushner, M. J., “Breakdown processes in metal halide lamps,” *Plasma Sources Science and Technology*, Vol. 12, 2003, pp. 8-21.
8. Deconinck, T., Mahadevan, S., and Raja, L. L., “Discretization of the Joule heating term in plasma discharge fluid models using unstructured meshes,” *Journal of Computational Physics*, in review.
9. Liou, M.-S. and Steffen, C. J., “A new flux-splitting scheme,” *Journal of Computational Physics*, Vol. 107, 1993, pp. 23-39.
10. Haselbacher, A. and Blazek, J., “Accurate and Efficient Discretizations of Navier-Stokes Equations on Mixed Grids,” *AIAA Journal*, Vol. 38, 2000, pp. 2094-2102.
11. Venkatakrishnan, V., “Convergence to steady state solutions of the Euler equations on unstructured grids with limiters,” *Journal of Computational Physics*, Vol. 118, 1995, pp. 120-130.
12. Lieberman, M. A., and Lichtenberg, A. J., *Principles of Plasma Discharges and Materials Processing*, John Wiley & Sons, New York, 1994.